redin Revista Facultad de Ingeniería, Universidad de Antioquia, No.110, pp. 86-98, Jan-Mar 2024

Experimental and numerical investigation of flat plate fins and inline strip fins heat sinks

Investigación experimental y numérica de disipadores de calor de aletas continuas y en tiras alineadas

William Denner Pires-Fonseca [1*] Carlos Alberto Carrasco-Altemani [1]

[1]Energy Department, School of Mechanical Engineering. Cidade Universitária, Campinas. R. Mendeleyev, 200 Cidade Universitária, 13083-860. Campinas, Brasil.

CITE THIS ARTICLE AS:

W. D. Pires-Fonseca and C. A. Carrasco-Altemani. "Experimental and numerical investigation of flat plate fins and inline strip fins heat sinks", *Revista Facultad de Ingeniería Universidad de Antioquia*, no. 110, pp. 86-98, Jan-Mar 2024. [Online]. Available: https://www.doi.org/10.17533/udea.redin.20230417

ARTICLE INFO:

Received: August 18, 2020
Accepted: April 10, 2023
Available online: April 10, 2023

KEYWORDS:

Experimental analysis; numerical analysis; heat sinks; cooling of electronic equipment

Análisis experimental; análisis numérico; disipadores de calor; enfriamiento de equipos electrónicos

ABSTRACT: The flow and heat transfer characteristics of two analogous heat sinks were obtained from laboratory experiments and compared to each other and to numerical simulations. One contained continuous straight fins, and the other inline strip fins, both cooled by forced airflow parallel to their base. The average airflow velocity in the interfin channels ranged from 4 to 20 m/s, corresponding to Reynolds numbers from 810 to 3,800. The measurements indicated that despite its smaller heat exchange area, the strip fins heat sink convective coefficient was larger enough to obtain a thermal resistance smaller than that of the continuous fins. Numerical simulations were performed to compare their results with the experiments. Two distinct fin treatments were used: one considered fins with no thickness, isothermal with the fins base temperature. The other considered the fins thickness and perfect thermal contact with the heat sink base. The Nusselt number simulation results for the continuous fins agreed within 3% with the measurements, but larger deviations were observed for the strip fins heat sink.

RESUMEN: Las características de flujo y transferencia de calor de dos disipadores de calor análogos se obtuvieron a partir de experimentos de laboratorio y se compararon entre sí y con simulaciones numéricas. Uno contenía aletas rectas continuas y el otro, aletas de tira en línea, ambas enfriadas por un flujo de aire forzado paralelo a su base. La velocidad promedio del flujo de aire en los canales entre aletas osciló entre 4 y 20 m/s, lo que corresponde a números de Reynolds de 810 a 3800. Las mediciones indicaron que a pesar de su menor área de intercambio de calor, el coeficiente de convección del disipador de calor de las aletas de tira era lo suficientemente grande como para obtener una resistencia térmica menor que la de las aletas continuas. Se realizaron simulaciones numéricas para comparar sus resultados con los experimentos. Se utilizaron dos tratamientos distintos para las aletas: uno consideró aletas sin espesor, isotérmicas con la temperatura base de las aletas. El otro consideró el grosor de las aletas y un perfecto contacto térmico con la base del disipador de calor. Los resultados de la simulación del número de Nusselt para las aletas continuas coincidieron en un 3% con las medidas, pero se observaron desviaciones mayores para el disipador de calor de las aletas en tira.

1. Introduction

The continuous increase of the heat flux from electronic components and devices presents a significant challenge to the industry in order to keep their temperature within the manufacturers' specifications for a reliable life cycle [1–3]. In order to overcome any electronic failures that may emerge from an undesirable temperature increase, a series of innovative cooling techniques have been developed, including the use of phase change materials, thermoelectric cooling, liquid cooling techniques, high conductive fillings and thermal interface materials [4–8]. In spite of all these efforts, forced convection air cooling still remains the most employed mechanism for the general cooling of electronic equipment. It is mainly so when the temperature control must be attained with

* Corresponding author: William Denner Pires-Fonseca
E-mail: fonsecawdp@gmail.com
ISSN 0120-6230
e-ISSN 2422-2844

DOI: 10.17533/udea.redin.20230417

minimum cost. In this case, atmospheric air is the cooling fluid, due to its availability, handling facility and dielectric properties.

Because of its thermal properties (relatively small specific mass and thermal conductivity), the forced convection air cooling is usually employed with finned heat sinks, in order to prevent higher temperatures. The fins increase the convective heat transfer area and they may increase the heat transfer coefficient, as well as the conductive and radiative heat losses from the electronic components. Among the heat sinks, that with straight fins of constant cross section is the simplest and the most widely encountered [9–17]. It is usually employed with a parallel forced airflow in the interfin channels and the base plate. From the flow entrance in these channels, there is a development of the velocity and thermal boundary layers, which increase the heat sink convective thermal resistance along the flow. This increase may be reduced by a partition of the continuous fins into strip fins of smaller length. The strip fins heat exchange area is reduced in comparison to the heat sink of the same size with continuous straight fins. This area reduction may, however, be compensated by an increase in the average heat transfer coefficient of the strip fins.

This eventual heat transfer enhancement has led to several studies presented in the literature. Sparrow *et al.* [18] proposed a numerical investigation of the laminar flow and heat transfer from channels with periodical strip fins along the flow direction. The numerical results were obtained for a range of Reynolds numbers and for several values of a dimensionless geometrical parameter. They indicated that the partition of a single longitudinal fin into smaller strip fins reduces the boundary layers growth and, thus, the strip fins convective thermal resistance.

Sparrow and Liu [19] compared numerical results for the convective heat transfer and the pressure drop for the laminar flow along continuous fins and strip fins with inline and staggered arrangements. Their results showed that for constant mass flow rate and heat transfer area, the strip fins thermal efficiency is considerably larger than that of the continuous fins. Their results also indicated that the staggered strip fins arrangement presented a better thermal performance than the inline arrangement. A numerical analysis of the comparative performance of the inline and staggered geometrical distribution of strip fins was performed by Al-Sallami *et al.* [20]. Their investigation included the effects of perforated fins to enhance convective heat transfer. Their results also indicated that the staggered fins arrangement gives a larger heat transfer rate, at the expense of a larger flow pressure drop. Ozturk and Tari [21] performed a numerical investigation of heat sinks with strip fins applied to the CPU of a computer. They investigated the effects of the number of fins and their distribution, as well as the fins material and the heat sink base thickness. They found that although they had different geometries, all of the heat sinks studied had similar thermal resistances. However, replacing aluminum with copper as the heat sink material improved the performance.

Other investigations were also performed with the purpose to optimize the geometrical parameters of the strip fins heat sinks. Teertstra *et al.* [22] developed an analytical model for predicting the heat transfer rate from heat sinks with inline strip fins. They indicated that for a range of Reynolds numbers ($40 < Re < 180$), the best configuration for the inline strip fins is with a ratio of fins spacing (S) to pitch (P) equal to (S/P) = 0.5 and for a ratio of fins pitch to baseplate length in the range $0.059 < P/L < 0.44$. Hong and Cheng [23] also presented numerical results to optimize the geometrical parameters of strip fins heat sinks. They indicated that there is an optimal strip length to minimize the flow pressure drop and that it is independent of both the heat transfer distribution on the heat sink base and its maximum temperature.

The numerical investigations, as those reported previously, are useful to predict the heat sink performance from their detailed information about the flow and temperature fields, for a specific heat sink configuration and operating conditions. Additional numerical results may also be easily obtained to represent the effects of changes in the heat sink size and operating conditions. Then, a heat sink prototype, considering distinct design purposes, may be selected from the numerical simulations. The actual thermal behavior of the prototype may then be measured in laboratory experiments.

This paper aims to present the results of an experimental investigation to compare the thermal and flow characteristics of two heat sinks, one with continuous fins and the other with inline strip fins, both cooled by forced airflow in the laboratory. Most investigations report results for the interfin flow in the laminar regime. There are two main reasons for this. One is that a larger flow pumping power is required as the interfin flow velocity increases and the other is that as the velocity increases in the interfin channels, there may appear an inconvenient noise, like a whistle, and this is not recommended for several applications due to hearing discomfort. In the present experimental investigation, the range of airflow velocities in the interfin channels was larger than it is usually found in the literature. The experimental results include the airflow pressure drop through the heat sinks, the average Nusselt number in the interfin channels, the convective thermal resistance and the effectiveness of both heat sinks. The numerical simulations were

performed with the computational software PHOENICS [24]. They were carried out for a three-dimensional domain consisting of a heat sink channel, assuming uniform velocity and temperature profiles at the channel entrance. The heat sink base was assumed to be an isothermal plate in perfect thermal contact with the fins. For the numerical simulations in the laminar regime, the equations of conservation of mass, *momentum* and energy were solved under steady-state conditions. For the turbulent regime, such equations were solved using an additional zero equation turbulence model (LVEL). The experimental results were compared with those from the numerical simulations.

2. Experimental investigation

Two similar aluminum heat sinks, one with a flat plate fins and the other with inline strip fins, as indicated in Figure 1, were tested in a laboratory. Each heat sink had 16 lines of fins with a height of 0.0113 m on a rectangular base of length L = 0.09 m and width W = 0.0415 m (other dimensions are indicated in Table 1). The tests were performed with a heat sink assembled in a rectangular duct in such a way that the fins base was flush mounted to the inner surface of one duct wall. The heat sink fins tips then touched the rectangular duct opposite wall, so that there was no top bypass. On both sides of the assembled heat sink, there was a lateral bypass with rectangular duct walls equal to one fins' spacing. The rectangular duct cross section was equal to (0.0452 x 0.0113) m, and its length was equal to 0.170 m. It was made from four 0.005 m thick Plexiglas plates connected by screws and sealed with silicone rubber.

Each heat sink was assembled 0.010 m from the duct entrance. The duct was connected, as indicated in Figure 2, to the front wall of a plenum box with a partition wall where a calibrated nozzle was installed to measure the airflow rate during the experimental tests. The airflow in the duct was provided in suction mode by a fan located outside the laboratory and connected by a duct with a flow control valve to the end wall of the plenum box.

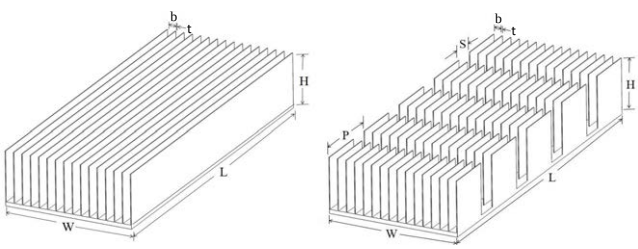

Figure 1 (a) flat plate fins heat sink and (b) strip fins heat sink

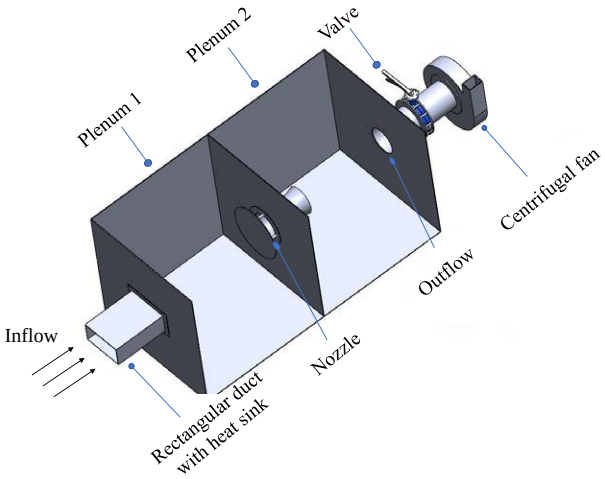

Figure 2 Illustration of an experimental apparatus

Table 1 Geometric parameters of heat sinks

Parameters	Values [mm]
L	90
H	14
W	41.5
P	19
S	5
b	1.86
t	0.86

Two distinct experimental tests were performed with each heat sink. One was to obtain the airflow pressure drop through the heat sink and the other was to obtain the thermal results. The flow pressure drop through the heat sinks was measured under steady, isothermal ambient conditions. The airflow rate in the duct was varied by means of the flow control valve in the tube downstream of the plenum box and it was measured by the flow pressure drop in the nozzle using an inclined manometer. The airflow pressure drop through the heat sink was measured by a differential pressure transducer (PX750-06DI, Omega Eng.). This pressure drop was that from the ambient air in the laboratory to a pressure tap located in the rectangular duct, 30 mm downstream of the heat sink. Two similar pressure drop measurements of the flow in the duct were performed. First, with the heat sink in the duct and then in the duct without the heat sink, that is, just the flow pressure drop in the plain duct. The results to be presented for the airflow pressure drop through the heat sink were obtained by subtracting the later measurement from the former. Thus, the present pressure drop results indicate the effect of the presence of the heat sink in the duct.

The thermal tests were also performed for each heat sink mounted in the same rectangular duct, under steady-state

conditions. The heating was accomplished by electric power dissipation in a plate resistance (16 Ω) with almost the same dimensions of the heat sink base. This plate was attached to the heat sink base with good thermal contact, employing a commercial thermal paste (Implastec). In these tests, the rectangular duct with one heat sink and the heating plate were thermally insulated by a 25 mm layer of polystyrene (k = 0.033 W/m.K). All the thermal tests were performed with the heat sink base temperature around 40°C. The electric power dissipation in the heating plate was provided by a dc power supply (Instrutherm FA-3005). It was obtained from the dc electric current and the voltage drop across the heating plate, measured by a digital multimeter (HP 34401A). The temperature measurements were obtained from type E thermocouples (Teflon-coated 0.254 x 10^{-3} m diameter wires from Omega Eng.). They were read by a digital temperature indicator (Omega Eng. DP41-TC), with a resolution of 0.1°C. The tested heat sinks and the duct were instrumented with eight thermocouples as follows. The rectangular heat sink base had three thermocouples located 2 mm below its surface, along a diagonal. The other five thermocouples were located at the duct entrance (1), on the heater plate (1), on the Plexiglas duct wall (2) and on the insulation layer (1).

Thirteen experimental tests were performed with each heat sink, encompassing a range of the average airflow velocities in the interfin channels from 4 m/s to 20 m/s. In each thermal test, a predetermined flow rate in the duct with a heat sink was adjusted by the flow control valve. Then, the electric power dissipation was set so that the heat sink base was around 40°C and all the thermocouples were read in time intervals of half an hour. The results from each test were obtained under steady-state conditions, assumed when all the temperature readings were within 0.1°C during a time interval of 30 minutes. The time interval to attain this condition was around three hours for each test.

2.1 Data reduction

In each experimental test, the air mass flow rate in the rectangular duct ($\dot{m}_d$) was the same as that in the long radius nozzle located in the plenum box. This nozzle was built according to ISO 5167, with an inner radius of 0.017 m and it had been previously calibrated to obtain a nozzle flow coefficient (K_b). From this coefficient, the mass flow rate was obtained by a standard procedure from the measurement of the flow pressure drop across the nozzle. When each heat sink (16 lines of fins) was inserted in the rectangular duct, the airflow was subdivided into 17 interfin channels with a rectangular cross section equal to the fins length and spacing. It was assumed that in each of these channels, the mass flow rate ($\dot{m}_c$) was equal to 1/17 of the duct mass flow rate ($\dot{m}_d$). From $\dot{m}_c$, the average airflow velocity in the interfin channels (V) was then obtained. It was used to define a Reynolds number based on the rectangular interfin channels hydraulic diameter (D_h), as in Equation (1).

$$Re_c = \frac{VD_h}{\nu} \tag{1}$$

The forced convective heat transfer from the heat sink to the airflow (q_{cv}) was evaluated by an energy balance on the heat sink under steady-state conditions. The electric power dissipation (P_d) in the plate resistance in contact with the heat sink base was not fully transferred from the heat sink to the airflow. Several thermal losses (q_l) were evaluated and their sum was subtracted from P_d. These losses included thermal radiation from the heat sink base and fins, conduction through the thermal insulation covering the rectangular duct, and conduction through the power and thermocouple wires. In all the tests, the estimated thermal losses were estimated to be less than 3% of the power dissipation P_d in the plate resistance. The energy balance to obtain q_{cv} was expressed by Equation (2).

$$q_{cv} = P_d - \Sigma q_l \tag{2}$$

From the convective heat transfer rate q_{cv}, the heat sink thermal resistance was obtained as in Equation (3).

$$R_{th} = \frac{(T_b - T_\infty)}{q_{cv}} \tag{3}$$

In this equation, T_b and T_∞ represent the heat sink base temperature and the airflow inlet temperature in the heat sink, respectively. The thermal resistance can be associated with a simple model [25] based on an average heat transfer coefficient, as in Equation (4).

$$R_{th} = \frac{1}{h^*(A_b + \eta_f A_f)} \tag{4}$$

The heat transfer coefficient (h^*) is based on the flow inlet temperature (T_∞) and the efficiency (η_f) was obtained considering the standard adiabatic fins tips model. The experimental values of R_{th} were obtained from Equation (3) and they were used in Equation (4) to obtain the heat transfer coefficients (h^*). This was an iterative process because the fin efficiency η_f depends on h^*. The results were expressed in non-dimensional form by a Nusselt number based on the interfin channels hydraulic diameter (D_h), as in Equation (5).

$$Nu = \frac{h^* D_h}{k} \tag{5}$$

The results of the present investigation have also considered the heat sinks as heat exchangers [26, 27]. In this approach, the heat sink convective heat transfer to the airflow was described as that of a heat exchanger by the effectiveness (ϵ) method, as presented in Equation (6).

$$q_{cv} = \dot{m} c_p \epsilon (T_b - T_\infty) \quad (6)$$

From Equations (3) and (6), the heat sink effectiveness may be expressed as in Equation (7).

$$\epsilon = \frac{1}{R_{th} \dot{m} c_p} \quad (7)$$

The heat sink base temperature (T_b) was considered isothermal, and thus, it was associated with the hot side of a heat exchanger with an infinite thermal capacity. In this case, the heat capacity ratio is equal to zero and the heat sink effectiveness (ϵ) is related [25] to the number of transfer units (NTU) by Equation (8).

$$\epsilon = 1 - exp(-NTU) \quad (8)$$

For the finned heat sinks, the number of transfer units NTU = $(\overline{h} \eta_0 A_t)/(\dot{m} c_p)$. In this definition, $\overline{h}$ is the average, over the channel length, heat transfer coefficient based on the flow local mixed mean temperature, η_0 is the overall finned surface efficiency and A_t is the total heat sink convective heat transfer area. Distinct heat sink designs may lead to distinct NTU values under similar flow conditions. Larger NTU values give rise to larger effectiveness, resulting in smaller heat sink thermal resistances.

2.2 Uncertainty analysis

A spreadsheet was developed in the EES (Engineering Equation Solver - F-Chart Software) program to evaluate the uncertainties of the experimental results based on the method of uncertainty propagation [28]. Considering a result S, obtained by n experimental measurements x_i, the uncertainty of S (denominated σ_S) can be evaluated by Equation (9):

$$\sigma_S = \sqrt{\sum_{i=1}^{N} \left(\frac{\partial S}{\partial x_i} \Delta x_i \right)^2} \quad (9)$$

The absolute or relative uncertainties of all measurements were specified, along with the nominal measurements of each test. The results and their uncertainties were then obtained for each experimental test performed. The absolute uncertainties for the readings of the inclined manometer, U-manometer and thermocouples were estimated according to Table 2. For the aluminum and air properties, relative uncertainties of 1% of the tabulated values were assumed. These uncertainties were inserted in the EES worksheet to obtain the uncertainty values for the air mass flow rate, the Reynolds number, the convective heat transfer rate and the airflow pressure drop.

Table 2 Values adopted for uncertainties

Variable	Uncertainties
Inclined manometer height [in alcohol]	0.005
U-Manometer height [mmca]	0.5
Thermocouple temperature [°C]	0.1
Barometric pressure [hPa]	5.0
Coefficient K of the nozzle [-]	0.02
Aluminum properties [%]	2.5
Air properties [%]	1.0

3. Numerical investigation

The experimental results of the average Nusselt number in the channels of both heat sinks were compared not only to each other, but also to results obtained from numerical simulations performed under steady-state conditions. Additional information obtained from the simulations will also be presented, in order to illustrate the flow and heat transfer in the heat sinks. Several physical simplifications were adopted in these simulations, as will be indicated in the following, and their effect will be reflected in the results to be presented.

For both heat sinks, i.e., for that with straight fins and also for that with strip fins, the simulations were performed for a single heat sink channel. It was assumed that the heat sink airflow rate was equally distributed into all the heat sink channels. It was also assumed, for the strip fins channel, that the flow at the entrance of the channel did not migrate to a neighbor channel, although this mixing may actually occur at the end of each strip fin. That was a necessary assumption to perform the simulations considering a single heat sink channel. Additional assumptions were a uniform flow velocity and temperature at the entrance of the numerical domain. Atmospheric air was assumed as the cooling fluid for both heat sinks, flowing parallel to their bases.

The conservation equations were solved by the finite volumes method to obtain the air velocity and temperature distributions in one interfin channel of each heat sink. The numerical results were compared to the experimental results previously obtained. In order to have a broader perspective on the present investigation, two distinct fin models were used in the simulations. The first fin model considered thin plate fins with no thickness, isothermal with the heat sink base temperature. The second model considered the actual fins' thickness and material, in perfect thermal contact with the heat sinks isothermal base. For the strip fins heat sink, for example, the numerical domain used for the simulations with the fin model with no thickness is indicated in Figure 3, and for the model with thick fins, it is indicated in Figure 4.

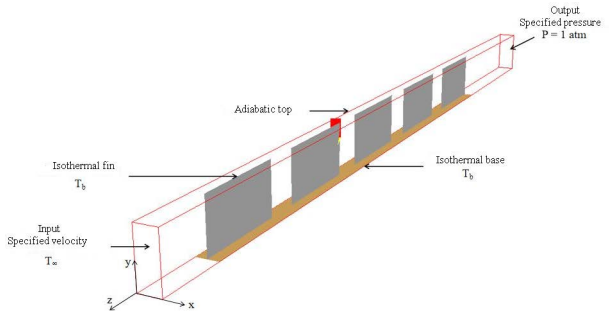

Figure 3 Numerical domain for the first fin model - isothermal plates with no thickness

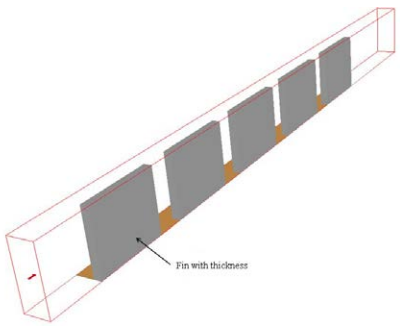

Figure 4 Numerical domain for the second fin model - thick non-isothermal fins

3.1 Simulations

The numerical simulations to obtain the heat sinks flow and heat transfer parameters were performed with the package PHOENICS [24]. The conservation equations of mass, *momentum* and energy were solved under steady-state conditions by three-dimensional simulations using the finite volumes method [29]. When the Reynolds numbers in the interfin channels (Re_c) were up to 2,300, the simulations were performed for laminar flows. For higher Reynolds numbers, the simulations were performed with the zero equation turbulence model LVEL [30] incorporated in the PHOENICS package. It employs a continuous universal velocity profile in the range from 0 $< y^+ <$ 100, described in the work of Spalding [31]. The LVEL model is indicated for the simulation of the flow in narrow passages and it evaluates the distances from the nodal points to the walls automatically, in order to obtain the velocity profile described in this work of Spalding. The transition to turbulence for rectangular ducts with abrupt entrance and the aspect ratios from 3 to 10 is reported in Hartnett *et al.* [32] for a duct Reynolds number around 2,500 to 2,800. The rectangular ducts of the plate fins heat sink used in this investigation had channels with an aspect ratio equal to 6.1. The conservation equations (continuity, RANS, and energy) were expressed by Equations (10) to (12):

$$\frac{\partial u_i}{\partial x_i} = 0 \tag{10}$$

$$\frac{\partial u_i u_j}{\partial x_j} = -\frac{1}{\rho}\frac{\partial p}{\partial x_i} + \frac{\partial}{\partial x_j}\left[\left(\frac{\partial u_i}{\partial x_j} + \frac{\partial u_j}{\partial x_i}\right)(\nu + \epsilon_M)\right] \tag{11}$$

$$\frac{\partial (u_i T)}{\partial x_i} = \frac{\partial}{\partial x_i}\left[\frac{\partial T}{\partial x_i}(\alpha + \epsilon_H)\right] \tag{12}$$

In these equations, the spatial coordinates are represented by x_i and x_j. The velocity components are indicated by u_i and u_j and the pressure and temperature are represented, respectively, by p and T. The fluid properties are indicated by (ρ) density, (ν) kinematic viscosity, and (α) thermal diffusivity. The turbulent diffusivities ϵ_M and ϵ_H were obtained from the LVEL turbulence model, assuming a turbulent Prandtl number (ϵ_M/ϵ_H) equal to one. The coupling between velocity and pressure in the transport equations was solved iteratively by the algorithm SIMPLEST, developed by Spalding [33]. The advective terms were interpolated by the hybrid scheme [34].

3.2 Modeling of the heat sink channels

The two fin models (thick and no-thickness fins) employed in this work gave rise to two distinct numerical domains for each heat sink, as shown in Figures 3 and 4 only for the strip fins. Figure 3 shows the numerical domain for the no-thickness fin model, considering a row of strip fins centered in the channel. The domain dimensions were equal to 1.85 mm in the x direction, 11.3 mm in the y direction and 130 mm along the z direction. The upstream fin was 10 mm downstream the flow entrance in the numerical domain, the same heat sink position in the experimental duct.

Figure 4 shows the numerical domain in the case of the thick non-isothermal fins. In this case, due to symmetry, the numerical domain comprised only half of the heat sink channel width. Similar to the experimental setup, the numerical domain, in this case, was 1.36 mm in the x direction, 11.3 mm in the y direction and 130 mm in the z direction. It contained only half of the fins thickness, i.e., 0.43 mm.

For the no-thickness fin model, a uniform surface temperature was imposed on the fins surfaces and on the heat sink base. For the second model, considering the fins thickness, a temperature was specified on the heat sink base. In this case, the fins were considered to have perfect thermal contact with the heat sink base and an adiabatic condition was imposed on their tips. Uniform velocity and temperature profiles were adopted for the air inflow in the numerical domain. The inlet velocity varied from 4

to 20 m/s, corresponding to a range of Re_c between 810 and 3,800. The airflow properties were considered at the average between the airflow inlet temperature (assumed at 18°C) and the average flow mixing temperature at the outlet section of the numerical domain. This value was usually around 20°C, so that the air properties in the simulations were taken as follows. Density: 1.204 kg/m^3, kinematic viscosity: 1.516×10^{-5}m^2/s, conductivity thermal: 0.02514 W/m.K, specific heat: 1,007 J/kg.K and number of Prandtl: 0.7. No radiation effects were considered in the simulations.

3.3 Numerical mesh

An investigation of the numerical mesh was carried out in order to obtain consistent results without a prohibitive simulation time and memory. The geometry of the inline strip fins, simulated with the thickness fin model was used in these tests. The uniform airflow entry velocity in the numerical domain was specified at 4 m/s, the lowest simulated value, corresponding to laminar flow. The tests started with a relatively coarse grid that was gradually refined, increasing the number of control volumes in each direction, as well as the mesh concentration near the walls. This procedure allowed the simulations to be performed with the largest channel width, so that the most refined mesh would be needed to obtain converged numerical results. The lowest velocity was employed in these tests in order to solve the laminar flow and energy equations without any additional model in the simulations.

The six investigated meshes are presented in Table 3, where Nx, Ny ,and Nz represent the number of control volumes, respectively, in the x, y, and z directions, and CV indicates the total number of control volumes in the computational domain. The tested meshes were refined in the vicinity of the duct walls and fins. To verify the independence of the numerical grid in the results, the mean Nusselt number (Nu) was used as a parameter. As indicated in Figure 5, a value of the mean Nusselt number was independent of the computational mesh when it contained more than 244,800 control volumes (mesh 5). However, with a mesh of 144,000 volumes (mesh 4) there was a deviation of only 1.5% in this results, which was considered acceptable and then used to obtain the numerical results. A microcomputer with a FX8350 processor (©Advanced Micro Devices, Inc.) with 8 physical cores, 16 GB of RAM and a video card with 1 GB of dedicated memory was used in the simulations. The average processing time for each test with the adopted mesh was around 15 minutes for the simulations in the laminar regime and 50 minutes for those in the turbulent regime. The corresponding number of iterations to attain the converged solution was around 600 and 1,800, respectively, for the laminar and the turbulent airflow regimes.

Table 3 Investigated meshes

Mesh	Nx	Ny	Nz	CV
1	10	15	35	5,250
2	20	30	51	30,600
3	30	40	80	96,000
4	30	60	80	144,000
5	40	60	102	244,800
6	80	120	204	1,958,400

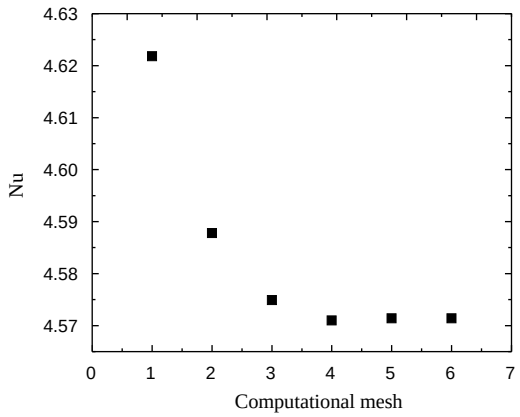

Figure 5 Change of the average Nusselt number with the computational mesh

4. Results and discussion

The experimental tests were performed with aluminum heat sinks with plate fins and inline strip fins, with the dimensions shown in Table 1, comprising each 16 parallel lines of fins. Each row of strip fins had five fins separated from each other with uniform spacing. The average airflow velocity in the interfin channels varied from 4 to 20 m/s. The corresponding interfin channels Reynolds number based on their hydraulic diameter was in the range from 810 to 3,800.

4.1 Pressure drop

The measured airflow pressure drop across the heat sinks is presented in Figure 6 as a function of the average airflow velocity in the interfin channels. These pressure drops for each heat sink were obtained from two sets of measurements of the flow pressure drop from the laboratory ambient air to a pressure tap located in the rectangular duct lower wall, 30 mm downstream the heat sink. The first set was obtained with the heat sink installed in the duct and the second, with the heat sink removed from the duct. The results presented in Figure 6 represent the difference between the first and the second sets for each heat sink. They indicate the flow pressure drop increase in the rectangular duct associated to the

presence of the heat sink. The test data show a monotonic increase of the flow pressure drop with the channels velocity. When comparing the two heat sinks, the airflow pressure drop for the strip fins heat sink is increasingly larger than that for the plate fins, indicating the need for larger fan power as the airflow velocity increases. It is also noticed that for low average flow velocities, in the range of 4 to 8 m/s, the pressure drop in the two heat sinks is practically the same, with a percentage difference of only 12%.

The experimental data points of the airflow pressure drop through the heat sinks were adjusted by quadratic functions, expressed by Equations (13) and (14), respectively, for the flat plate fins (ΔP_{pf}) and inline strip fins heat sink (ΔP_{sf}). These equations, as well as Equations (15-20), were obtained using the least-squares method, implemented in the Curve Fitting toolbox and coded in MATLAB. The quality of the adjustments is given by the coefficients of determination (R^2) that are presented for each case.

$$\Delta P_{pf} = 1.0833V^2 + 6.6068V + 17.043 \qquad R^2 = 0.9995 \tag{13}$$

$$\Delta P_{sf} = 0.7651V^2 + 2.239V + 1.779 \qquad R^2 = 0.9983 \tag{14}$$

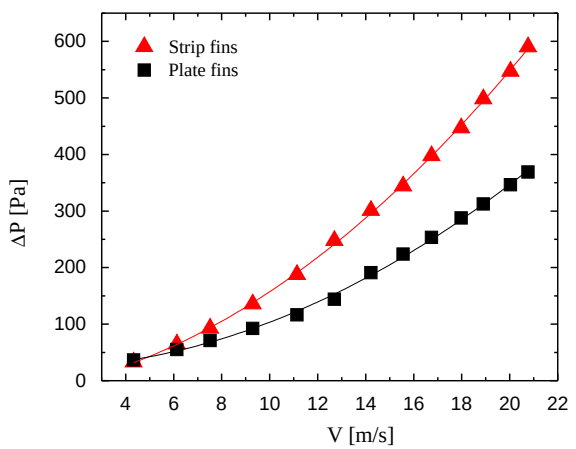

Figure 6 Pressure drop of the airflow through the heat sinks

4.2 Average Nusselt number

The rate of heat transfer by forced convection from the heat sinks tested in the laboratory to the airflow was obtained as indicated by Equation (2). From this rate, it was possible to obtain the experimental data for the average heat transfer coefficient h^* (using the flow inlet temperature as a reference) obtained from Equation (4). This coefficient was used to evaluate the average Nusselt number, as defined by Equation (5).

The results for the average Nusselt number for both heat sinks are shown in Figure 7 as a function of the airflow Reynolds number in the channel. Note that for both heat sinks, the values increase with the Reynolds number in the channel. When analyzing the plate fins heat sink, the results indicate two distinct regions. Up to a Reynolds number value around 2,400, the flow was characterized as laminar and for Reynolds values above 3,000, the flow was assumed turbulent. Equations (15) and (16) show correlations for the average Nusselt number as a function of the Reynolds number in each channel for the plate fins heat sink, respectively for the laminar and turbulent flow regimes. This subdivision is coherent with the literature on the critical Reynolds number in rectangular channels with abrupt entrance, presents more accurate correlations as compared to a single correlation for all the data and reflects the physics of the fluid flow in these channels.

For the inline strip fins heat sink, a single correlation was adjusted for all the experimental data (Equation 17). This behavior of the average Nusselt number reflects the complex flow and convective heat transfer in the channels with inline strip fins. The strip fins in these channels induce the flow to separate at the downstream end of each fin and to start new boundary layers at the downstream strip fin, and so on. They must induce turbulent flow at low channel Reynolds number, as indicated by the single correlation encompassing all the data.

$$Nu_{pf} = 0.112Re_c^{0.52}; \quad 810 < Re_c < 2,400 \qquad R^2 = 0.9949 \tag{15}$$

$$Nu_{pf} = 0.002Re_c^{1.03}; \quad 3,000 < Re_c < 3,800 \qquad R^2 = 0.9946 \tag{16}$$

$$Nu_{sf} = 0.028Re_c^{0.77}; \quad 810 < Re_c < 3,800 \qquad R^2 = 0.9947 \tag{17}$$

The flat plate heat sink channels have a length of about 28 hydraulic diameters. In order to attain a thermally developed condition in the investigated laminar range of $810 < Re_c < 2{,}400$, these channels should have from 36 to 108 hydraulic diameters [25, 32]. Thus, Equation (15) represents results for the simultaneous entrance region in laminar flow. For $3{,}000 < Re_c < 3{,}800$, the entrance length for turbulent flow usually requires a length from 20 to 40 channel hydraulic diameters, so that Equation (16)

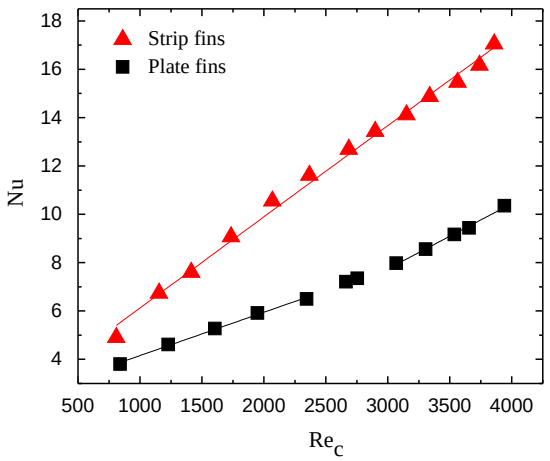

Figure 7 Heat sinks average Nusselt number

also represents a correlation for the entrance region in a turbulent flow. For the flow in the strip fins heat sink, open channels were associated with the space between consecutive rows of strip fins. Each strip fins acts a barrier with an abrupt entrance in these channels and thus, they induce a transition to turbulent flow at smaller Reynolds numbers. Equation (17) was expressed for the channels formed by consecutive rows of strip fins, as a single correlation for the entire range of the Reynolds number.

4.3 Convective thermal resistance

The experimental results for the heat sinks convective thermal resistance, defined by Equation (3), are presented in Figure 8 and they show a typical decrease as the average airflow velocity in the interfin channels increases. This result reflects the convective heat transfer increase with the airflow rate in the interfin channels, as was indicated in Figure 7.

These results show that in spite of the strip fins heat sink smaller heat transfer area, the average heat transfer coefficient is larger enough to give rise to a smaller thermal resistance in the investigated range of the Reynolds number. It should be kept in mind, however, that the strip fins heat sink demands a larger fan power for the same airflow velocity.

Equations (18), (19) and (20) show, respectively, the correlations for the plate fins heat sink (laminar and turbulent flow regimes) and for the inline strip fins heat sink thermal resistances.

$$R_{th(pf)} = 1.9V^{-0.5} \qquad R^2 = 0.9983 \tag{18}$$

$$R_{th(pf)} = 7.4V^{-1} \qquad R^2 = 0.9991 \tag{19}$$

$$R_{th(sf)} = 2.4V^{-0.75} \qquad R^2 = 0.9993 \tag{20}$$

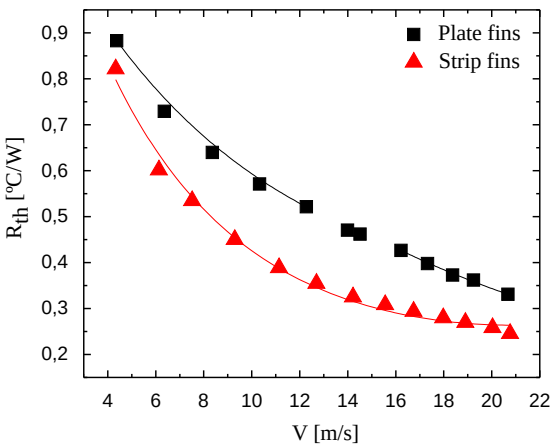

Figure 8 Heat sinks thermal resistance

4.4 Treatment of the heat sinks as heat exchangers

In the treatment of heat sinks as heat exchangers, the thermal resistance is inversely proportional to their effectiveness, as presented by Equation (7). In the experimental tests, the two heat sinks were subjected to the same range of air flow rates and thus, the comparison of the two heat sinks effectiveness provides a comparison of their thermal resistances.

The experimental results obtained for the effectiveness (ϵ) of the two heat sinks, treated as heat exchangers, are shown in Figure 9. For the same range of airflow rate, the strip fins heat sink operates with higher effectiveness than the plate fins heat sink. These results reflect the fact that the average convective coefficients are higher for the strip fins heat sink.

For both heat sinks, the NTU decreases with increasing airflow rate, thus causing a reduction in their effectiveness (ϵ). Comparatively, the strip fins heat sink presents a more

effective thermal design than the plate fins heat sink. For this heat sink to operate as effectively as the strip fin heat sink, it should operate in a lower range of air flow rate, thus increasing the NTU and the effectiveness values (ϵ).

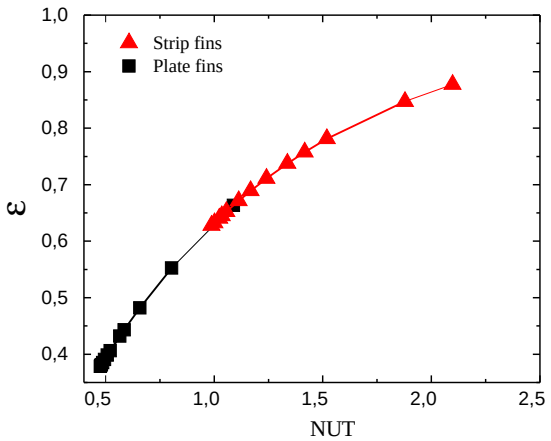

Figure 9 Effectiveness of the heat sinks as a function of the number of transfer units

4.5 Uncertainties of the experimental results

The uncertainties of the experimental results were estimated as described in section 2.2, for the airflow pressure drop, the average airflow velocity, the average Nusselt number, the Reynolds number, and the convective thermal resistance. The results obtained are presented in Table 4.

Table 4 Propagated values of relative uncertainties

Variable	Lowest $\dot{m}$ [kg/s]	Highest $\dot{m}$ [kg/s]
ΔP	5.3%	1.0%
V	4.6%	3.7%
Nu	2.9%	3.0%
Re	5.2%	4.6%
R_{th}	1.2%	1.2%

5. Numerical results

5.1 Plate fins heat sink

The numerical airflow temperature distribution in a plane parallel to the base of a flat plate fin is presented in Figure 10, considering the no-thickness fin model, when Re_c = 3,800. As expected, the airflow temperature increases both downstream the duct and also in the vicinity of the fin.

A comparison between the experimental and the numerical results for the average Nusselt number for the plate fin is shown in Figure 11. The numerical results were obtained from both fin models - with negligible fin thickness (1^{st} model) and with thick fins (2^{nd} model). The experimental data are those already presented in Figure 7 for the plate fins and they are reproduced here by the symbols only. The numerical simulations performed with the thick fin model are are physically more realistic and they presented Nusselt number results closer to the experimental data. There was a deviation of around 2% for the Reynolds number Re_c in the range from 810 to 2,300 (laminar regime) and about 3% for the range between 2,500 and 3,800 (turbulent regime). For the simulations with the no-thickness fin model, the results presented similar trends, but with larger deviations from the experimental data, as shown in Figure 11. They varied from 3% to 8% in the laminar regime and were around 9% in the turbulent regime.

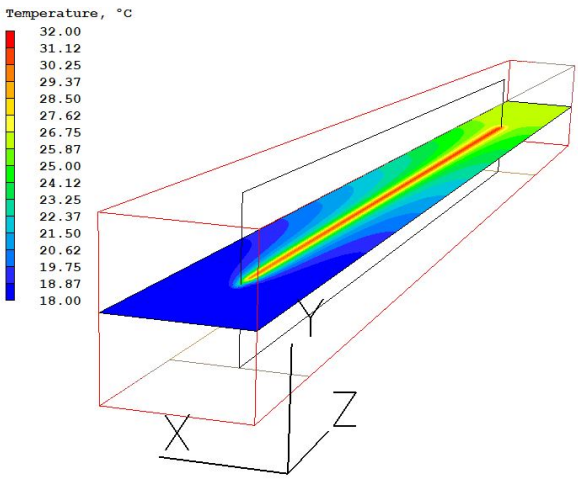

Figure 10 Numerical temperature distribution for the plate fins heat sink using the first fin model (Re_c = 3800)

5.2 Strip fins heat sink

The numerical airflow temperature distribution in a plane parallel to the base of a row of strip fin is presented in Figure 12, for the first fin model (no thickness), when Re_c = 3,800. The airflow temperature increases in the vicinity of the five strip fins and also in the downstream direction. The simulations were also performed for the thick fins model.

For the strip fins, the flow simulation is quite more complex due to the interrupted boundary layers growth at the end of each fin. In the present simulations, the x-boundaries of the numerical domain presented in Figure 12 were

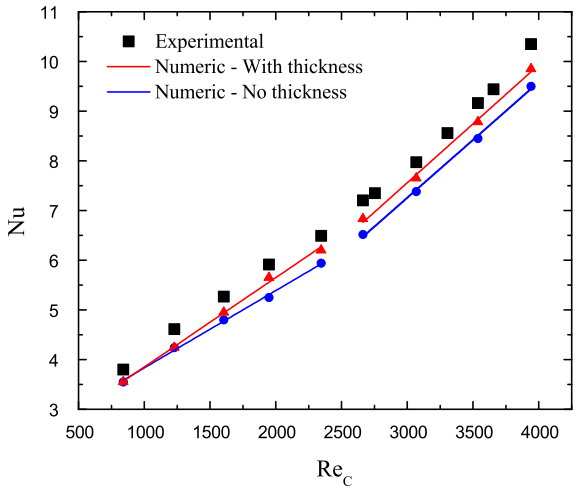

Figure 11 Nusselt number results from the experiments and the simulations for the plate fins heat sink

specified as symmetry planes, but this assumption may be subject to further investigation in the future. Thus, it may be anticipated that in this case the numerical results for the average Nusselt number in the fin channel will not be as comparable to the experiments as they were in the case of the flat plate fins.

In the simulations with the first fin model (no thickness), the flow was assumed in the laminar regime for $Re_c <$ 2,300 and in the turbulent regime for $Re_c >$ 2,500. When the second fin model (thick fin) was used, two distinct sets of simulations were performed over the entire Reynolds number range. For the first set the flow was assumed in the laminar regime, while the second set, it was assumed in the turbulent regime.

The numerical and experimental results for the average Nusselt number for the strip fins' channel are compared in Figure 13. The experimental results are the same as those from Figure 7 and they are indicated just by the symbols. The numerical results for the first fin model were obtained from simulations considering either laminar flow ($Re_c <$ 2,300) or turbulent flow ($Re_c >$ 2,500) and in both regimes the predictions were below the experimental values. For the second fin model (thick fins), the numerical results from the laminar flow assumption were also below the experimental values, but closer than those from the first fin model. The simulations for the turbulent flow assumption presented Nu results above the experimental values. These results indicate a complex flow around the strip fins, where turbulence may arise in the flow separations and re-attachments at each strip fin. The deviations with the first fin model were from 7% to 21% when the flow was in the laminar regime and from 17% to 21% in the turbulent regime. When the second fin model (thick fin) was adopted in the simulations, the deviations from the experimental results were from 1% to 6% below the experimental results when the entire flow was simulated in the laminar regime and they were between 22% and 37% above the experimental results when the flow was assumed turbulent over the entire Re_c range.

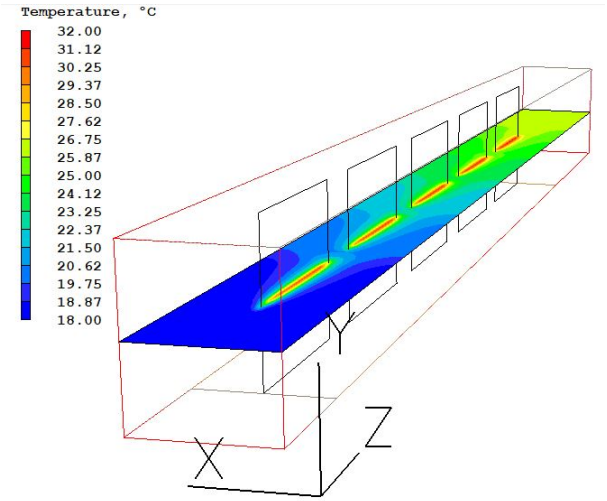

Figure 12 Numerical temperature distribution for the strip fins heat sink using the first fin model (Re_c = 3800)

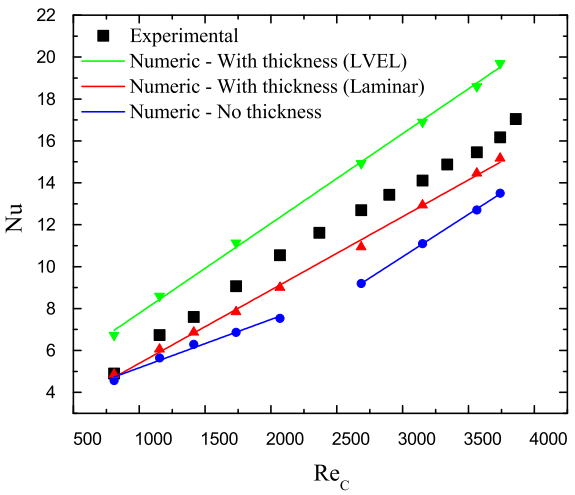

Figure 13 Nusselt number results from the experiments and the simulations for the strip fins heat sink

6. Conclusions

Laboratory experiments were carried out to obtain the airflow pressure drop and the forced convection heat transfer from two aluminum heat sinks, one with flat plate fins and the other with inline strip fins. Both heat sinks were mounted with no top bypass, but with a lateral bypass equal to one fin spacing on both sides in a rectangular duct. The experiments were carried out under steady-state conditions for an average airflow velocity in the interfin channels in the range from 4 to 20 m/s. This corresponded to a Reynolds number based on their hydraulic diameter in the range from 810 and 3,800, a range for which experimental data are scarce and the physics of the flow is not completely understood for the strip fins heat sink. In addition, numerical simulations for both heat sinks were performed in the PHOENICS package, assuming two fin models, one with isothermal fins of negligible thickness and the other with the actual fin thickness, for comparisons of the numerical with the experimental results. All the simulations were performed under steady-state conditions.

The experimental results indicated that the airflow pressure drop across the inline strip fins heat sink was always higher than that across the plate fins heat sink. The difference was small for the lowest flow velocities in the fins channels, but increased sharply with the velocity. This showed that the flow through the inline strip fins heat sink requires a greater fan power than through the flat plate fins heat sink.

The results of the thermal tests showed that the strip fins heat sink presented larger average heat transfer coefficients than the plate fins heat sink. They were about 25% larger for the lowest channel flow Reynolds number and about 41% larger for the highest. Despite the strip fins smaller heat transfer area, their heat transfer coefficient was larger enough so that they presented a smaller thermal resistance than the plate fins heat sink.

When the heat sinks were considered as heat exchangers, the strip fins heat sink effectiveness was distinctively higher than that of the plate fins heat sink. This result indicated that the strip fins heat sink presented a better thermal design under the tested conditions. It required, however, larger airflow pumping power, mainly in the highest range of the tested airflow velocity in the interfin channels.

The present experimental investigation was important to obtain reliable and useful information to compare the thermal behavior of two similar aluminum heat sinks, one with flat plate fins and the other with inline strip fins. The investigation was carried out in a higher airflow velocity in the interfin channels than it is usually found in the literature. The numerical thermal results were obtained employing two fin models with a commercial CFD package. There was a reasonable agreement with the experiments for the flat plate fins, but for the strip fins, with more complex flows, the comparison was not as good, indicating that further investigation is still needed.

7. Declaration of competing interest

We declare that we have no significant competing interests including financial or non-financial, professional, or personal interests interfering with the full and objective presentation of the work described in this manuscript.

8. Funding

The support of FAPEMA (Fundação de Amparo à Pesquisa e ao Desenvolvimento Científico e Tecnológico do Maranhão), in the form of a Scholarship to the first author, is deeply appreciated.

9. Author contributions

Conceptualization: William Fonseca and Carlos Altemani. Experiments and data processing: William Fonseca and Carlos Altemani. Paper preparation: William Fonseca and Carlos Altemani.

All authors participated fully in the preparation of this manuscript.

10. Data available statement

The authors confirm that the data supporting the findings of this study are available within the article [and/or] its supplementary materials.

References

[1] S. P. Gurrum, S. K. Suman, Y. K. Joshi, and A. G. Fedorov, "Thermal issues in next-generation integrated circuits," *IEEE Transactions on device and materials reliability*, vol. 4, no. 4, pp. 709–714, 2004.

[2] H. E. Ahmed, B. Salman, A. S. Kherbeet, and M. Ahmed, "Optimization of thermal design of heat sinks: A review," *International Journal of Heat and Mass Transfer*, vol. 118, pp. 129–153, 2018.

[3] Z. He, Y. Yan, and Z. Zhang, "Thermal management and temperature uniformity enhancement of electronic devices by micro heat sinks: A review," *Energy*, vol. 216, p. 119223, 2021.

[4] M. Hajmohammadi, V. A. Abianeh, M. Moezzinajafabadi, and M. Daneshi, "Fork-shaped highly conductive pathways for maximum cooling in a heat generating piece," *Applied thermal engineering*, vol. 61, no. 2, pp. 228–235, 2013.

[5] P. Hopton and J. Summers, "Enclosed liquid natural convection as a means of transferring heat from microelectronics to cold plates," in *29th IEEE Semiconductor Thermal Measurement and Management Symposium*. IEEE, 2013, pp. 60–64.
[6] H. M. Ali, A. Arshad, M. Jabbal, and P. G. Verdin, "Thermal management of electronics devices with pcms filled pin-fin heat sinks: a comparison," *International Journal of Heat and Mass Transfer*, vol. 117, pp. 1199–1204, 2018.
[7] A. Arshad, M. Jabbal, P. T. Sardari, M. A. Bashir, H. Faraji, and Y. Yan, "Transient simulation of finned heat sinks embedded with pcm for electronics cooling," *Thermal Science and Engineering Progress*, vol. 18, p. 100520, 2020.
[8] R. Kalbasi, "Introducing a novel heat sink comprising pcm and air-adapted to electronic device thermal management," *International Journal of Heat and Mass Transfer*, vol. 169, p. 120914, 2021.
[9] S. Churchill and R. Usagi, "A general expression for the correlation of rates of transfer and other phenomena," *AIChE Journal*, vol. 18, no. 6, pp. 1121–1128, 1972.
[10] P. Teertstra, M. Yovanovich, and J. Culham, "Analytical forced convection modeling of plate fin heat sinks," *Journal of Electronics Manufacturing*, vol. 10, no. 04, pp. 253–261, 2000.
[11] H. Jonsson and B. Moshfegh, "Modeling of the thermal and hydraulic performance of plate fin, strip fin, and pin fin heat sinks-influence of flow bypass," *IEEE Transactions on Components and Packaging Technologies*, vol. 24, no. 2, pp. 142–149, 2001.
[12] M. Shaeri and M. Yaghoubi, "Thermal enhancement from heat sinks by using perforated fins," *Energy conversion and Management*, vol. 50, no. 5, pp. 1264–1270, 2009.
[13] W. Al-Sallami, A. Al-Damook, and H. Thompson, "A numerical investigation of the thermal-hydraulic characteristics of perforated plate fin heat sinks," *International Journal of Thermal Sciences*, vol. 121, pp. 266–277, 2017.
[14] S. Chingulpitak, H. S. Ahn, L. G. Asirvatham, and S. Wongwises, "Fluid flow and heat transfer characteristics of heat sinks with laterally perforated plate fins," *International Journal of Heat and Mass Transfer*, vol. 138, pp. 293–303, 2019.
[15] A. A. Hussain, B. Freegah, B. S. Khalaf, and H. Towsyfyan, "Numerical investigation of heat transfer enhancement in plate-fin heat sinks: Effect of flow direction and fillet profile," *Case Studies in Thermal Engineering*, vol. 13, p. 100388, 2019.
[16] B. Freegah, A. A. Hussain, A. H. Falih, and H. Towsyfyan, "Cfd analysis of heat transfer enhancement in plate-fin heat sinks with fillet profile: Investigation of new designs," *Thermal Science and Engineering Progress*, vol. 17, p. 100458, 2020.
[17] A. Tariq, K. Altaf, S. W. Ahmad, G. Hussain, and T. Ratlamwala, "Comparative numerical and experimental analysis of thermal and hydraulic performance of improved plate fin heat sinks," *Applied Thermal Engineering*, vol. 182, p. 115949, 2021.
[18] E. Sparrow, B. Baliga, and S. Patankar, "Heat transfer and fluid flow analysis of interrupted-wall channels, with application to heat exchangers," 1977.
[19] E. Sparrow and C. Liu, "Heat-transfer, pressure-drop and performance relationships for in-line, staggered, and continuous plate heat exchangers," *International Journal of Heat and Mass Transfer*, vol. 22, no. 12, pp. 1613–1625, 1979.
[20] W. Al-Sallami, A. Al-Damook, and H. Thompson, "A numerical investigation of thermal airflows over strip fin heat sinks," *International Communications in Heat and Mass Transfer*, vol. 75, pp. 183–191, 2016.
[21] E. Ozturk and I. Tari, "Forced air cooling of cpus with heat sinks: A numerical study," *IEEE transactions on components and packaging technologies*, vol. 31, no. 3, pp. 650–660, 2008.
[22] P. Teertstra, J. Culham, and M. Yovanovich, "Analytical modeling of forced convection in slotted plate fin heat sinks," *ASME-PUBLICATIONS-HTD*, vol. 364, pp. 3–12, 1999.
[23] F. Hong and P. Cheng, "Three dimensional numerical analyses and optimization of offset strip-fin microchannel heat sinks," *International Communications in Heat and Mass Transfer*, vol. 36, no. 7, pp. 651–656, 2009.
[24] D. B. Spalding, "Phoenics. cham," *Multiphase Science and Technology*, vol. 6, no. 1-4, 2009.
[25] T. L. Bergman, F. P. Incropera, D. P. DeWitt, and A. S. Lavine, "Fundamentals of heat and mass transfer," *John Wiley & Sons*, 2011.
[26] R. L. Webb, "Heat exchanger design methodology for electronic heat sinks," 2007.
[27] R. J. Moffat, "Modeling air-cooled heat sinks as heat exchangers," in *Twenty-Third Annual IEEE Semiconductor Thermal Measurement and Management Symposium*. IEEE, 2007, pp. 200–207.
[28] H. W. Coleman and W. G. Steele, "Experimentation, validation, and uncertainty analysis for engineers," *John Wiley & Sons*, 2018.
[29] H. K. Versteeg and W. Malalasekera, "An introduction to computational fluid dynamics: the finite volume method," *Pearson education*, 2007.
[30] D. Agonafer, L. Gan-Li, and D. Spalding, "The lvel turbulence model for conjugate heat transfer at low reynolds numbers," *Application of CAE/CAD Electronic Systems, ASME*, vol. 18, pp. 23–26, 1996.
[31] D. Spalding, "A single formula for the law of the wall," *Journal of Applied Mechanics*, vol. 28, no. 3, pp. 455–458, 1961.
[32] J. P. Hartnett, J. C. Y. Koh, and S. T. McComas, "A comparison of predicted and measured friction factors for turbulent flow through rectangular ducts," *Journal of Heat Transfer*, vol. 84, pp. 82–88, 1962.
[33] D. Spalding, "Mathematical modelling of fluid-mechanics, heat-transfer and chemical-reaction processes," *A Lecture Course, Imperial College CFDU Report*, 1980.
[34] D. B. Spalding, "A novel finite difference formulation for differential expressions involving both first and second derivatives," *International Journal for Numerical Methods in Engineering*, vol. 4, no. 4, pp. 551–559, 1972.